Environment and Natural Resources Journal

Volume 22
Issue 3
2024

Phenolated Alkali Lignin/Magnetite Composite as an Adsorbent for Methyl Violet 6B in Wastewater

Mary Sheenalyn P. Rodil*, Corazon D. Sacdalan, Rissabell R. Robero, Maria Evytha L. Salinas, and Trixie N. Santander

Technological University of the Philippines, Manila, Philippines

ARTICLE INFO

Received: 20 Sep 2023
Received in revised: 2 May 2024
Accepted: 8 May 2024
Published online: 20 May 2024
DOI: 10.32526/ennrj/22/20230256

Keywords:
Adsorption kinetics/ Dye kemoval/ Isotherm models/ Optimization/ Reusability/ Thermodynamic

*** Corresponding author:**
E-mail:
marysheenalyn_rodil@tup.edu.ph

ABSTRACT

Methyl violet 6B (MV6B), found in wastewater, poses hazardous effects to aquatic ecosystems and human health; therefore, it must be removed immediately. In response, this study pioneered the development of a dye adsorbent by incorporating phenolated alkali lignin (PAL) into magnetite (Fe_3O_4), offering a solution for MV6B removal. Lignin was extracted from coconut husk through alkali extraction, chemically modified using phenolation, and integrated onto the magnetite surface. SEM and FTIR spectroscopy were used to characterize the adsorbent, and various parameters were optimized, along with evaluations of the adsorption kinetics and isotherm models, as well as the adsorbent's reusability. PAL was successfully deposited onto the magnetite based on the characterization. The experimental results revealed that the optimal conditions for the removal of MV6B using PAL/Fe_3O_4 composite are pH 4, a temperature of 313 K, a dosage of 0.10 g PAL/Fe_3O_4 per 15 mL of MV6B, and a contact time of 150 minutes. MV6B's equilibrium removal rate was 95.1%, with an adsorption capacity at equilibrium of 6.42 mg/g. The adsorption of MV6B followed a pseudo-second-order kinetic model and the Freundlich model isotherm. A thermodynamic study showed that the adsorption process was spontaneous and exothermic. PAL/Fe_3O_4 was highly reusable after three cycles without the need for desorption. Hence, this study has demonstrated that the PAL/Fe_3O_4 adsorbent is practical, economical, and efficient for wastewater treatment.

1. INTRODUCTION

Widespread industrialization and urbanization have led to an upsurge in groundwater and surface water pollution, which has become a top priority and a global crisis. This environmental crisis is exacerbated by the presence of dyes derived from industrial processes such as paper production, textile manufacturing, tanning operations, and paint industries. According to a World Bank report, the textile industry is responsible for between 17% and 20% of water contamination during the textile finishing and dyeing processes (Saini, 2017). As an effluent, these dyes can discharge in an aquatic environment from 2% for basic dyes to 50% for reactive dyes (Sharma et al., 2021). These dyes pose a threat not only to the integrity of wastewater and the environment but also to the balance of marine ecosystems and the well-being of the communities living in close proximity. Even at low concentrations, these dyes wield the potential to inflict significant and lasting harm upon the environment. The complex chemical structures and synthetic origins of many dyes used in industry make them resilient and difficult to remove.

One of the standard dyes heavily used by different industries is methyl violet 6B (MV6B). MV is a carcinogenic organic dye with long-lasting deleterious effects that pose hazards to humans, marine life, and the environment (Foroutan et al., 2019). MV has been classified as a hazardous recalcitrant substance, exhibiting limited biodegradability.

Citation: Rodil MSP, Sacdalan CD, Robero RR, Salinas MEL, Santander TN. Phenolated alkali lignin/magnetite composite as an adsorbent for methyl violet 6B in wastewater. Environ. Nat. Resour. J. 2024;22(3):257-269. (https://doi.org/10.32526/ennrj/22/20230256)

Conventional wastewater treatment systems are unable to effectively remove MV from the wastewaters, resulting in its dispersal into the environment (Casas et al., 2009). Various methods of removing dyes have been studied in order to reduce the adverse effects on the environment. These consist of membrane filtering, solvent extraction, biofilm utilization, coagulation-flocculation, bacterial treatment, electrochemical oxidation, and photocatalytic degradation. However, some of these methods can be expensive, energy-intensive, lead to the formation of secondary pollutants and require careful disposal of the generated sludge.

Due to its simple design, low cost, wide applicability, effectiveness and minimal environmental impact, another method used to clean wastewater contaminated with dyes is the utilization of adsorbents. Numerous analyses determined that polymeric adsorbent is effective in elimination of the differents dyes (Bensalah, 2024). Lignin is one kind of polymer capable of treating dye-contaminated wastewater. By altering, carbonizing, and compositing lignin, numerous researchers have produced a variety of lignin-derived adsorption materials, with potential uses in the wastewater treatment industry (Wang et al., 2022). In this recent study, lignin was modified through phenolation and magnetite was incorporated for faster magnetic separation. This process can lead to a novel lignin-based material, the phenolated alkali lignin/magnetite (PAL/Fe_3O_4) composite. Its ability to adsorb aqueous MV6B was evaluated, analyses of kinetic models, isotherm models and thermodynamic parameters were also carried out.

2. METHODOLOGY

2.1 Fabrication of phenolated alkali lignin/ magnetite (PAL/Fe_3O_4) composite

Alkali lignin is extracted using 123 g of coconut husk, which was air-dried, crushed into powder, and sieved through a 60-mesh filter. A mixture of 7.5% (w/v) NaOH solution and coconut husk powder in a 1:10 (w/v) ratio was prepared and refluxed for 1.5 h at 90±2°C. A cloth was used to filter the warm refluxed mixture. The filtrate was then cooled to room temperature. Following the cooling process, the filtrate, which appeared as a black liquor, was acidified using 2 M and 0.50 M H_2SO_4 until the pH reached a value of 2. The precipitate was filtered and repeatedly rinsed with distilled water until the pH became neutral, then dried (Panamgama and Peramune, 2018).

To synthesize the PAL, 9 g of extracted lignin and 36 g of phenol were dissolved in 90 mL of a 72% H_2SO_4 solution and continuously stirred for 6 h at 60°C. To dilute the H_2SO_4 to a 3% concentration, 2,070 mL of distilled water was added to the mixture, which was then heated for an additional hour at 125°C. The PAL was subsequently centrifuged at 10,000 rpm for 10 min. After being washed three times with distilled water, the PAL was dried for 6 h at 105°C.

For integration of Fe_3O_4 onto the surface of PAL, 18.2 g of $FeCl_3 \cdot 6H_2O$ and 12.6 g of $FeSO_4 \cdot 7H_2O$ were dissolved in 100 mL water and heated until the temperature reached 90°C (Benhalima et al., 2023a). Subsequently, 30 mL of 26% NH_4OH and 3 g of PAL in 600 mL of distilled water were added to the mixture. The pH was adjusted to 10 using 2 M and 0.10 M NaOH. The mixture was stirred at 300 rpm for 30 min at 80°C. The resulting PAL/Fe_3O_4 composite was subjected to centrifugation at 10,000 rpm for 10 min, followed by three rinses with distilled water, and finally, oven-dried at 50°C.

2.2 Characterization of phenolated alkali lignin/ magnetite (PAL/Fe_3O_4) composite

The surface morphology of the PAL/Fe_3O_4 composite underwent examination through scanning electron microscopy, with a voltage of 10.0 kV and a magnification of 10.6 mm × 500 and 10.0 k SE (Hitachi Model- SU3800; Tokyo, Japan). Fourier Transform Infrared Spectroscopy (Shimadzu IRTracer-100; Kyoto, Japan) in the wave number region from 400 cm^{-1} to 4,000 cm^{-1} was applied to analyze the alkali lignin, PAL, and PAL/Fe_3O_4 composite, giving evidence on chemical bond rearrangements and structural modifications.

2.3 Optimization of parameters in the adsorption of MV using PAL/Fe_3O_4 composite

Initially, the pH of 15 mL of a 45 mg/L MV6B solution was adjusted to levels 4, 6, 8, and 10 using 0.10 M HCl and 0.10 M NaOH. Afterward, 0.15 g of PAL/Fe_3O_4 composite adsorbent was introduced into each solution for 30 min. The adsorbent was subsequently isolated with a magnet, and the final MV6B concentration was determined at 592 nm using a UV-Vis spectrophotometer (UH5300 spectro-photometer; Tokyo, Japan). Next, under optimal pH conditions, four flasks each containing 15 mL of a 45 mg/L MV6B solution and 0.15 g of PAL/Fe_3O_4 were heated at a temperature of 293 K, 303 K, 313 K, and 323 K. After heating and reaching equilibrium, the

adsorbent was separated, and the MV6B concentration was measured as previously described. Following this, while maintaining the optimal pH and temperature, the study investigated the effect of varying the dosage of PAL/Fe_3O_4 composite (0.05 g, 0.10 g, 0.15 g, and 0.20 g). Each dosage was added to 15 mL of the 45 mg/L MV6B solution. Lastly, under the optimal conditions of pH, temperature, and dosage, 15 mL of a 45 mg/L MV6B solution was exposed to varying contact times, ranging from 5 min to 150 min. After each specified time interval, the adsorbents were separated, and the absorbance of the aqueous solution was recorded. The adsorption capacity at equilibrium (qe, mg/g) and the removal efficiency R (%) were calculated from the following Equations (1) and (2), respectively:

$$q_e = \frac{C_o - C_f}{w} \times V \quad (1)$$

$$\% R = \frac{C_o - C_f}{C_o} \times 100 \quad (2)$$

Where; C_o and C_f stand for the initial and final concentrations of the adsorbate (mg/L), V represents the volume of the solution (L), w is the mass of the adsorbent (g), and % R symbolizes the percentage of removal (Benhalima and Ferfera-Harrar, 2019).

2.4 Adsorption kinetic study

The adsorption of MV6B using PAL/Fe_3O_4 composite was investigated within 5 min to 150 min at optimal pH, temperature, and adsorbent dosage. The data underwent kinetic study, employing both the pseudo-first order (PFO) and pseudo-second order (PSO) models, following Equations (3) and (4), respectively.

$$\ln (q_e - q_t) = \ln q_e - K_1 t \quad (3)$$

$$\frac{t}{q_t} = \frac{1}{K_2 q_e^2} + \frac{t}{q_e} \quad (4)$$

Where; q_e represents the adsorption capacity at equilibrium (mg/g), q_t stands for adsorption capacity at time t (mg/g), K_1 denotes the rate constant of the PFO model (min^{-1}), and K_2 symbolizes the rate constant of the PSO model (min^{-1}) (Benhalima et al., 2017).

2.5 Adsorption isotherm model

MV6B solutions spanning concentrations from 20 mg/L to 90 mg/L were prepared. Subsequently, 15 mL of each solution was ombined with 0.10 g PAL/Fe_3O_4. These mixtures were conditioned at pH 4 and a temperature of 313 K. Following this, the equilibrium concentrations were ascertained and subjected to analysis utilizing the Langmuir, Freundlich, and Temkin isotherm models, following Equations (5), (6), and (7), respectively.

$$\frac{C_e}{q_e} = \frac{C_e}{q_m} + \frac{1}{K_L q_m} \quad (5)$$

$$\log (q_e) = \log(K_F) + \frac{1}{n} \log (C_e) \quad (6)$$

$$q_e = B \ln (K_T) + \frac{RT}{b} \ln C_e \quad (7)$$

Where; C_e represents the concentration of adsorbate at equilibrium (mg/L), while q_e denotes the adsorption capacity at equilibrium (mg/g). The parameter q_m refers to the maximum adsorption capacity of the adsorbent (mg/g). K_L was used to symbolize the Langmuir isotherm constant (L/mg), and K_F represents the Freundlich isotherm constant (L/mg). The variable n signifies the degree of adsorption favorableness, b represents the heat of adsorption (J/mol), and B stands for the Temkin constant (RT/b), where R is the universal gas constant (8.314 J/mol·K), T is the absolute temperature (K), and K_T signifies the Temkin constant (Benhalima et al., 2017).

2.6 Thermodynamic study

To obtain an understanding of how temperature affects the adsorption process, the thermodynamic parameters, such as Gibbs free energy change (ΔG°), standard enthalpy change (ΔH°), and standard entropy change (ΔS°), were evaluated. These were done at a temperature of 293 K, 303 K, and 313 K. The following equations were utilized in the calculation of these parameters:

$$\Delta G^\circ = -RT \ln K_d \quad (8)$$

$$\ln K_d = -\frac{\Delta H^\circ}{RT} + \frac{\Delta S^\circ}{R} \quad (9)$$

Where; K_d represents the concentration ratio of the MV6B adsorbed to the MV6B remained in solution at equilibrium. R is the universal gas constant (8.314 J/mol·K), while T is the absolute temperature in Kelvin. To find the values of ΔH° (in kJ/mol) and ΔS° (in J/mol·K), respectively, ln K_d was plotted linearly against (1/T). The slope and intercept of the resulting graph were computed (Benhalima et al., 2017).

2.7 Reusability of phenolated alkali lignin/ magnetite (PAL/Fe_3O_4) composite

After the first adsorption of MV6B using 0.10 g of PAL/Fe_3O_4 under optimal conditions, the adsorbent was recovered using magnets and dried. The reusability of PAL/Fe_3O_4 was evaluated through three successive cycles without employing a desorption process. The the removal efficiency R (%) were calculated from Equation 2.

3. RESULTS AND DISCUSSION

3.1 Fabrication of phenolated alkali lignin/ magnetite composite (PAL/Fe_3O_4) composite

Figure 1 illustrates the fabricated alkali lignin (a), phenolated alkali lignin (PAL) (b), and the PAL/magnetite composite (PAL/Fe_3O_4) (c) utilized in this study. Coconut husk underwent alkaline lignin extraction using a 7.5% NaOH (w/v) solution to increase the pore volume and surface area of lignin. The resulting solid residue was separated from the black liquor and processed to obtain 77 g of deep brown alkali lignin from an initial 123 g sample. This alkali lignin was phenolated in an acidic medium at an elevated temperature, involving the condensation of its aromatic rings with phenol to increase the phenolic hydroxyl groups (Taleb et al., 2020). The resulting phenolated alkali lignin (PAL) served as a multidentate ligand for binding to iron oxide through coordination. This binding transformed the iron oxide surface, enhancing PAL's attachment. Incorporating magnetite into the composite was done to functionalize the adsorbent, improving adsorption efficiency and enabling faster magnetic separation (Liu et al., 2020; Touihri et al., 2021).

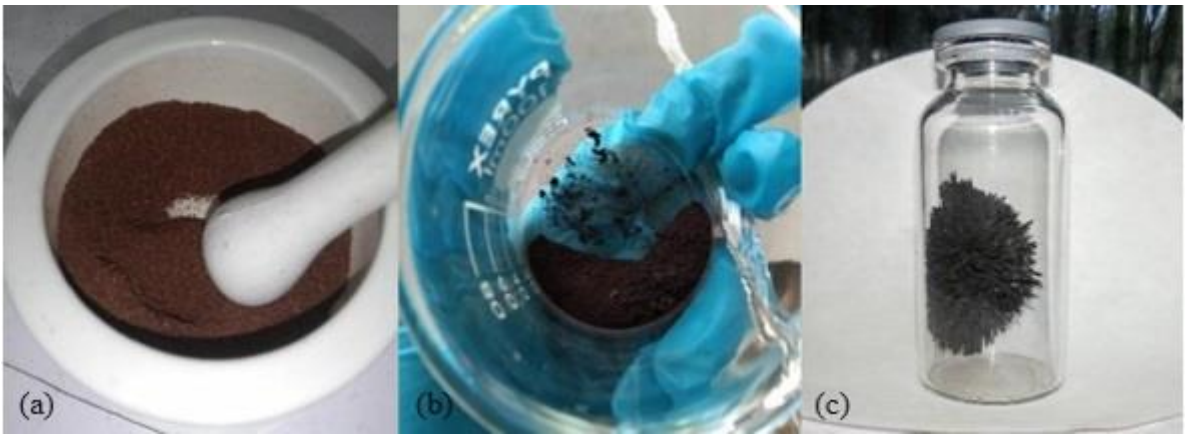

Figure 1. Fabricated of (a) alkali lignin, (b) PAL, and (c) PAL/Fe_3O_4 composite

3.2 Characterization of phenolated alkali lignin/ magnetite Composite (PAL/Fe_3O_4) composite

3.2.1 Fourier transform infrared (FTIR) spectroscopy

Figure 2 presents the FTIR spectrum of the adsorbent, which comprises lignin, PAL, and PAL/ Fe_3O_4.

In the lignin spectrum, O-H stretching vibrations are present at 3,321 cm^{-1}. The spectrum exhibits characteristic C=C stretching vibrations at 1,604 cm^{-1}, indicative of aromatic rings within the lignin structure. Peaks in the region around 1,035 cm^{-1} represent aromatic C-H in-plane deformation (Chaudhari, 2016). In contrast, phenolated alkali lignin (PAL) retains the aromatic rings found in unmodified lignin, displaying strong absorption peaks in the 1,500-1,600 cm^{-1} range, attributable to C=C stretching vibrations within the aromatic rings. Compared to lignin spectra, PAL exhibits a broader absorption band at 3,232 cm^{-1}, supporting the increased presence of phenolic functional groups, which are products of the phenolation process, in PAL (Younesi-Kordkheili and Pizzi, 2021). Distinct peaks between 1,593 cm^{-1} and 1,500 cm^{-1} in the spectra represent the bending vibrations of hydroxyl groups (OH) in lignin. The C-O stretching vibrations of these groups, appearing as a band at 1,118.71 cm^{-1}, serve as their defining characteristics. Peaks in the 2,850-2,916 cm^{-1} range, corresponding to C-H stretching vibrations, particularly in aliphatic and methoxy groups, indicate that the lignin has undergone changes. Since aliphatic groups in lignin are unusual, the development of these peaks in the spectra is likely due to the influence of modifications.

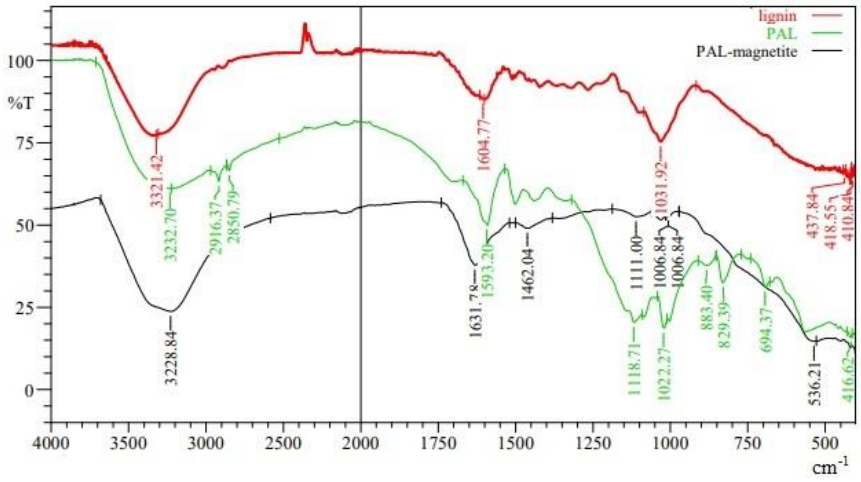

Figure 2. FTIR spectra of alkali lignin, PAL, and PAL/Fe_3O_4 composite

In the PAL/Fe_3O_4 spectrum, a spectral band at 3,228 cm^{-1} is broader than in PAL, confirming the presence of a substantial O-H group. Distinct peaks are evident at 1,006 cm^{-1} and 1,111 cm^{-1}, which can be directly attributed to the elongation of C-O bonds within the phenolic hydroxyl group. These peaks serve as clear indicators of the chemical interaction between PAL and magnetite. The spectrum also exhibits a peak at 536 cm^{-1}, signifying the intense vibration of Fe-O bonds originating from magnetite. This pronounced Fe-O band underscores the presence of magnetite in the composite (Benhalima et al., 2023a).

3.2.2 Scanning electron microscopy (SEM)

Figure 3 displays the SEM images showcasing the surface morphology of PAL/Fe_3O_4 at magnifications of 500x and 10000x.

The images show that the adsorbent exhibits a rough surface, with some particles displaying a granulated appearance and compact grain structures of varying sizes. This heterogeneous structure of the adsorbent particles can be attributed to the uneven adhesion of PAL to magnetite, resulting in the creation of numerous adsorption sites, which are important to improve the adsorbent's capacity and effectiveness when interacting with dye molecules (You et al., 2022).

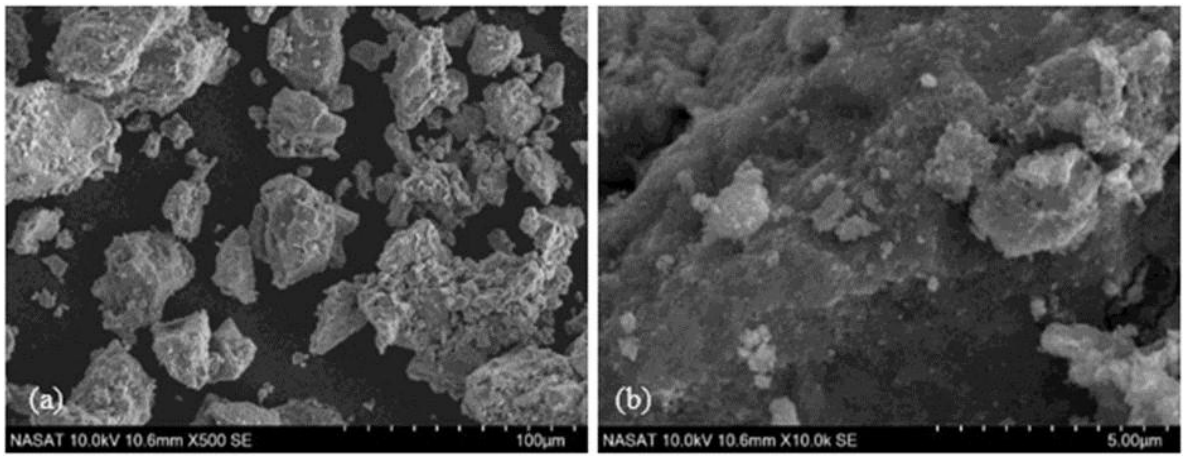

Figure 3. SEM images of PAL/Fe_3O_4 with magnifications of (a) 500x and (b) 10000x

3.3 Parameter optimization for the removal of MV6B via adsorption

Figure 4 displayed the results of the parameter optimization for the removal of MV6B.

The adsorption efficiency values decrease with rising pH from 4 to 10. At low pH, MV6B, and PAL undergo protonation due to the high concentration of H^+ ions in the acidic environment. However, given that phenolated alkali lignin is a polymeric substance with a complex structure, their interaction does not primarily depend on electrostatic attraction between their charged moieties (Meng et al., 2020). The

interaction can be driven by hydrophobic interactions facilitated by their aromatic structures, along with strong π-π stacking interactions. Additionally, despite their positive charges, potential hydrogen bonding between functional groups such as hydroxyl (-OH) groups in PAL and nitrogen atoms in MV6B and charge-induced interactions can contribute to their binding. At basic pH, alterations in solubility, conformation, and aromatic ring alignment in PAL and MV6B can reduce the exposure of hydrophobic regions, disrupt π-π stacking interactions and weaken hydrogen bonding. However, the adsorption efficiency persists at high level because of the strong affinity of MV6B onto negatively charged adsorbents. In alkaline media, the phenolate ions are generated and thus enhance electrostatic attraction affinity toward the cationic dye.

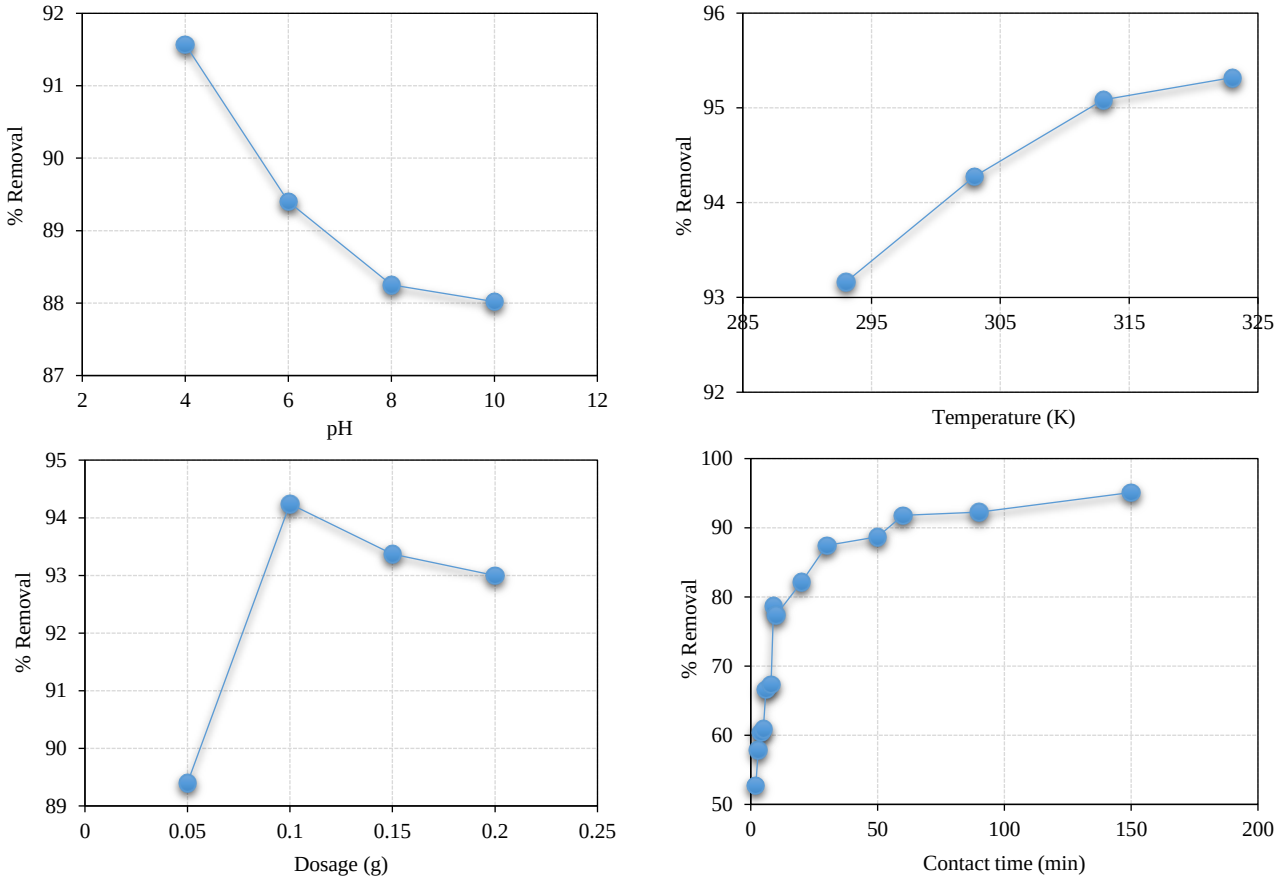

Figure 4. The effects of pH, temperature, dosage, and contact time on the adsorption of MV6B using PAL/Fe_3O_4

The adsorption efficiency increases as the temperature rises from 293 K to 323 K, indicating that adsorption is an endothermic reaction. The adsorption at 313 K and 323 K is not significantly different, suggesting that the adsorption of MV6B plateaus after the temperature surpasses 313 K. Furthermore, the most efficient adsorption was observed at 0.10 g PAL/Fe_3O_4. As the amount increases beyond 0.10 g, the capacity to adsorb decreases due to the minor agglomeration of the adsorbents. This agglomeration covers the active sites, preventing the binding of MV6B (Chen and Chen, 2018).

Under ideal conditions of pH, temperature, and PAL/Fe_3O_4 dosage, the optimal contact time for MV6B adsorption is 150 min. The adsorption efficiency increases as time progresses, followed by a plateau in adsorption efficiency, which results from the saturation of available adsorption sites by MV6B.

3.4 Adsorption kinetics

Figure 5 depicts the linear fitting of pseudo-first-order model and the pseudo-second-order kinetic model of the adsorption of MV6B using PAL/Fe_3O_4 composite. The relevant parameters of the models including equilibrium rate constant, adsorption capacity at equilibrium and correlation coefficients are shown in Table 1.

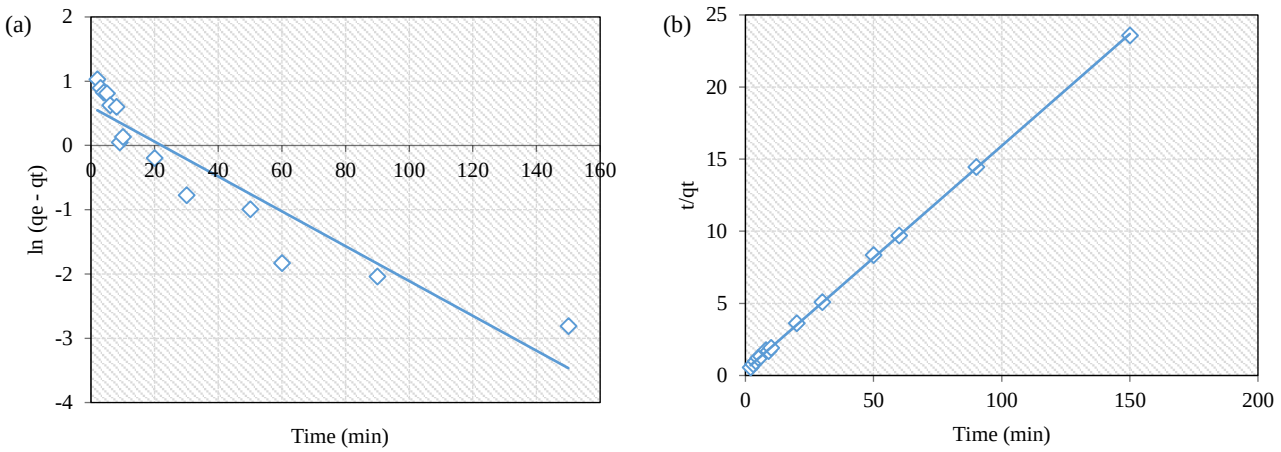

Figure 5. Linear fitting of the (a) pseudo-first and (b) pseudo-second-order kinetic model of the adsorption of methyl violet using PAL/Fe_3O_4 composite

Table 1. Parameters of pseudo-first and pseudo-second-order kinetic model of the adsorption of methyl violet using PAL/Fe_3O_4

Parameters	Pseudo-first-order	Pseudo-second-order
Equilibrium rate constant, K	-1.75×10^{-4}/min	6.04×10^{-2} g/mg·min
q_e, experimental	6.42 mg/g	6.42 mg/g
q_e, calculated	1.95 mg/g	6.44 mg/g
R^2	0.913	0.999

It could be clearly seen that pseudo-second-order model best described the adsorption kinetics with higher correlation coefficient (R^2=0.999) versus the pseudo-first-order model (R^2=0.913), indicating a chemisorption process. The kinetics study implied chemical interactions between the MV6B and PAL/Fe_3O_4 surface, as shown in Figure 6, characterized by electrostatic attraction, hydrophobic interactions facilitated by their aromatic structures, along with strong π-π stacking interactions and hydrogen bonding. Chemical adsorption assumes a dominant role in magnetic lignin compared to diffusion (Fang et al., 2021; Benhalima et al., 2023b; Benhalima et al., 2024).

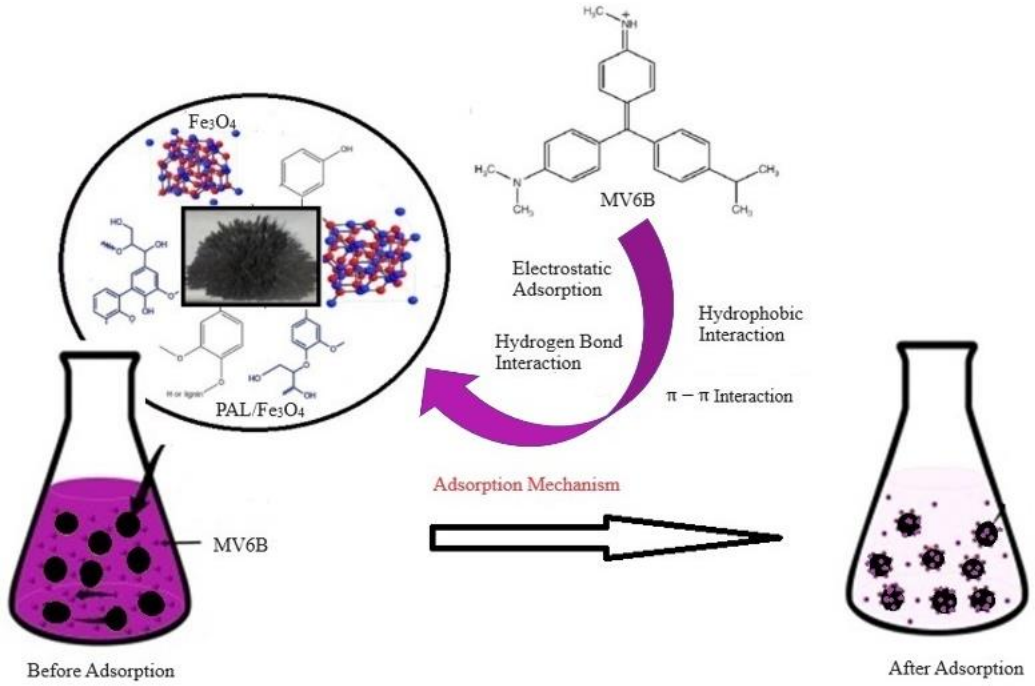

Figure 6. Adsorption mechanism of MV6B on PAL/Fe_3O_4 composite adsorbent

3.5 Adsorption isotherm

An adsorption isotherm defines the interaction between the adsorbate and the adsorbent and provides the capacity of the adsorbent to adsorb. The Langmuir isotherm model is used to describe monolayer adsorption, which occurs when all available active sites are occupied, reaching maximum adsorption and saturation (Liu et al., 2019). The Temkin isotherm predicts that the heat of adsorption for all molecules reduces linearly with increasing coverage (Ringot et al., 2007). On the other hand, the Freundlich isotherm gives an expression for the surface heterogeneity, the exponential distribution of active sites, and their energy (Ayawei et al., 2015). Figure 7 shows the linear fitting of the Langmuir, Temkin, and Freundlich isotherm model of the adsorption of MV6B using PAL/Fe_3O_4 composite while Table 2 provides the parameters for each model such as maximum monolayer adsorption capacity (q_m), binding energy (B_T), equilibrium constant (K_L or K_T), and the Freundlich constant (K_F), along with correlation coefficients (R^2).

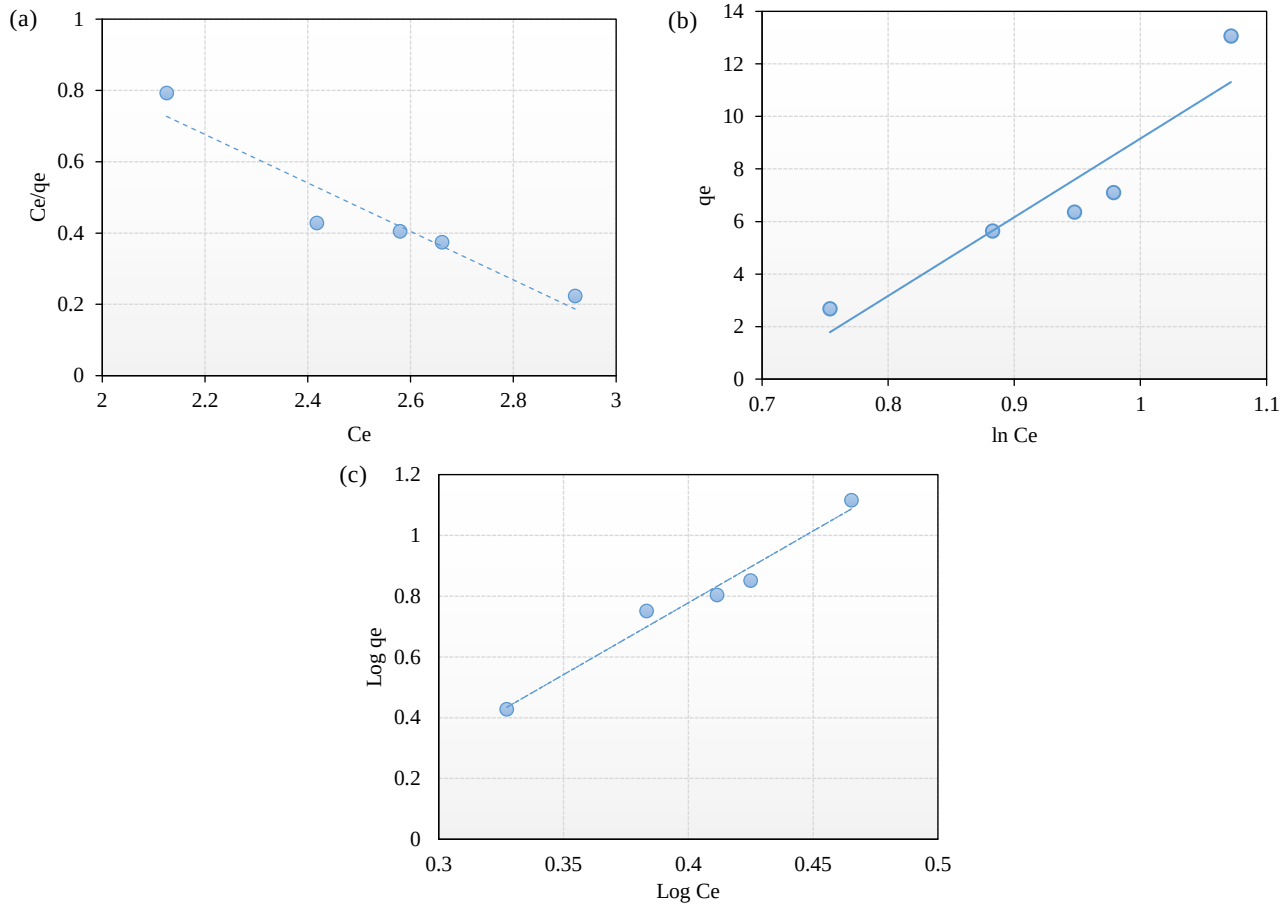

Figure 7. Linear fitting of the (a) Langmuir, (b) Temkin, and (c) Freundlich isotherm model of the adsorption of MV6B using PAL/Fe_3O_4

Table 2. Parameters of Langmuir, Temkin, and Freundlich isotherm model

Langmuir isotherm	Temkin isotherm	Freundlich isotherm
q_m (mg/g)=-1.470	B_T (J/mol)=29.96	n=0.212
K_L (L/mg)=-0.312	K_T (L/mg)=0.4994	K_F (L/mg)=0.0771
R_L=-0.0917	R^2=0.872	R^2=0.971
R^2=0.909		

The Langmuir isotherm model employs the separation factor (R_L) to assess the favorability of an isotherm. When $0<R_L<1$, it is considered favorable; when $R_L>1$, it is unfavorable; $R_L=1$ indicates linearity, and RL=0 implies irreversibility (Ayawei et al., 2017). As indicated in Table 2, the R_L value obtained is -0.0917, signifying that the Langmuir isotherm for MV6B adsorption using PAL/Fe_3O_4 is unfavorable.

This is supported by a correlation coefficient of 0.9099. On the other hand, the Temkin model's calculated R^2 was 0.8718, thus cannot adequately describe MV6B's adsorption. The positive BT values for MV6B (29.96 J/mol) demonstrate an endothermic reaction, with a K_T value of 0.4995 L/mg.

In the Freundlich model, the adsorption phenomenon is considered favorable when n<1, unfavorable when n>1, linear adsorption when n=1 and irreversible when n=0 (Chiban et al., 2011). The adsorption favorability value, n, is 0.212 which implies favorable adsorption. The Freundlich model best described the adsorption isotherm with higher correlation coefficient (R^2=0.971) versus the other two models, indicating that the adsorption sites are non-identical. Furthermore, Freundlich model describes multilayer adsorption, which means the quantity of adsorbate adsorbed escalates with an increase in solution concentration. The determined adsorption capacity constants exhibited a value of 0.0771 L/mg.

3.5 Thermodynamic Study

The thermodynamic parameters which provide understandings into the energetics of the adsorption of MV6B on PAL/Fe_3O_4 were presented in Table 3.

Table 3. The thermodynamic parameters for MV6B adsorption on PAL/Fe_3O_4 at different temperatures

Temperature (K)	K_d	ln K_d	Thermodynamic parameters		
			ΔG° (kJ/mol)	ΔH° (kJ/mol)	ΔS°(J/mol·K)
293	1.362463	0.309294	-0.75382753	1.60	5.76
303	1.647635	0.499341	-1.258534079		
313	1.934874	0.660042	-1.718439123		

The negative values of ΔG° and the positive value of ΔH° indicate that the adsorption of the MV6B was spontaneous and endothermic. The spontaneity increase from 293 to 313 K, signifying more driving forces and thus greater adsorption capacity at higher temperatures. In chemisorption process, this suggests that the formation of chemical bonds between the MV6B and PAL/Fe_3O_4 is energetically favorable, leading to the adsorption of the species onto the surface. Positive ΔS° values indicate that the MV6B become more disordered upon adsorption onto the PAL/Fe_3O_4 surface.

3.6. Reusability of PAL/Fe_3O_4 composite in the adsorption of MV6B

The reusability of PAL/Fe_3O_4 shown in Figure 8 was evaluated through repeated adsorption cycles without desorption. The optimal conditions, determined from the evaluated parameters, are as follows: C_o=45 mg/L, pH=4, and a dosage of 0.10 g/15 mL at 313 K.

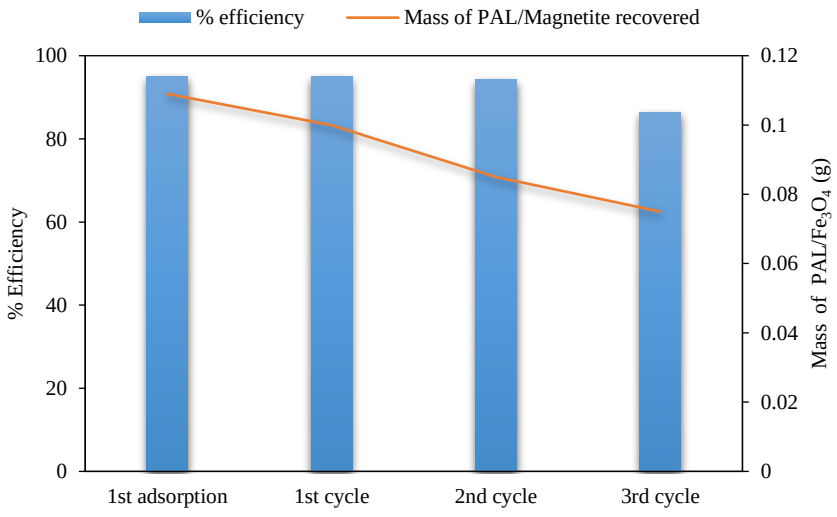

Figure 8. Reusability of PAL/Fe_3O_4 composite in the adsorption of MV6B dye

The adsorption capacity of PAL/Fe_3O_4 experienced a minimal decline between the first and second adsorption cycles. However, by the third cycle, the percent removal decreased to 86.53%, due to weight loss of the adsorbent during recovery and the potential saturation of adsorption sites owing to prior adsorption processes. As PAL is modified by Fe_3O_4, it can be recovered by magnetic substances after adsorption and has good reuse performance. Similarly, the study of Canbaz (2023), highlights the potential of magnetite-containing adsorbents as reusable and environmentally friendly alternatives in wastewater treatment. The results are align with the Freundlich model, which predicts efficient dye uptake without a significant desorption process. The Freundlich model suggests multilayer adsorption, which could explain the absence of desorption. Thus, PAL/Fe_3O_4 exhibits impressive reusability while retaining its adsorption capacity, making it a practical and cost-effective option for wastewater treatment.

Figure 9 displays the UV-visible analysis of the MV6B solution before and after adsorption, providing insights into the repeatability of the process. Following the adsorption process, reduction in the intensity of the 592 nm peak is evident, signifying a decrease in the concentration of MV6B within the solution. There is no significant shift in the position of the absorption peak, which suggests that there was no substantial degradation of MV6B during the adsorption process.

The MV6B after adsorption was also analyzed using Shimadzu IRTracer-100 FTIR to ensure the absence of secondary pollution including phenol, result was shown in Figure 10.

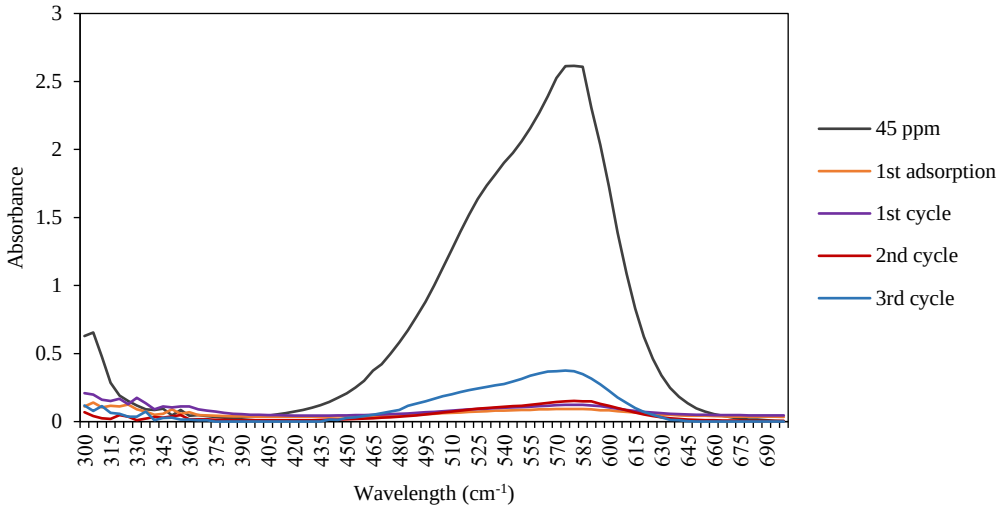

Figure 9. UV-visible spectrum of MV6B after several adsorptions at 592 nm

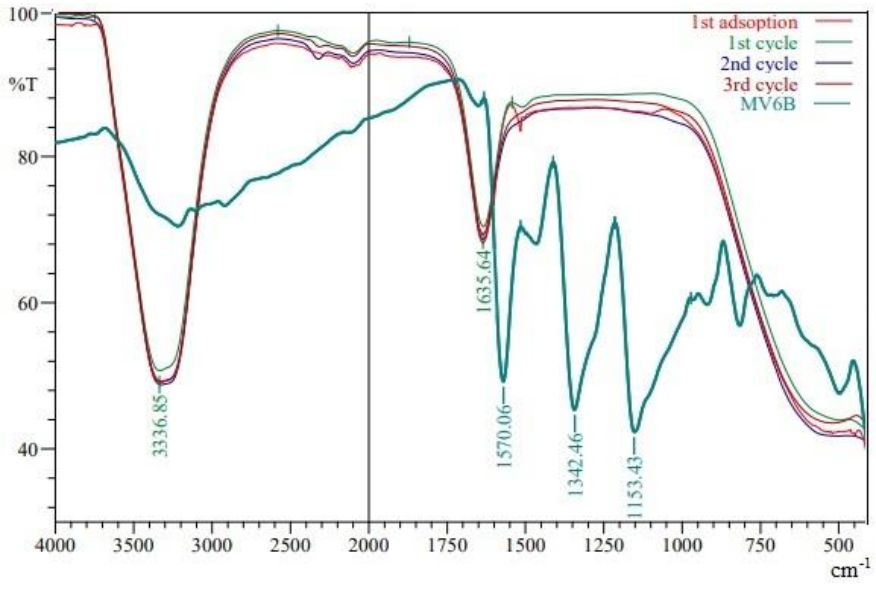

Figure 10. FTIR spectra of MV6B after adsorption using PAL/Fe_3O_4

The IR peaks indicated the presence of water. The peaks around 3,400 cm^{-1} indicates strong absorption due to the stretching of the O-H bonds in water molecules. The peaks that appears around 1,600-1,700 cm^{-1} corresponds to the bending motion of the water molecule. No bending vibration of C-H bonds in the aromatic ring appeared at 1,300-1,500 cm^{-1}, indicating the absence of phenol.

3.7 Comparison of adsorption capacities of various adsorbents for the removal of MV dye

A comparative study of adsorbents synthesized in this study with various types of adsorbents documented in the literature for methyl violet removal is presented in Table 4.

Based on the data provided in Table 4, the prepared composites in this study have lower adsorptive capacity as compared with other adsorbents for methyl violet dye exclusion. This discovery emphasizes the need for more research to optimize the present composites' adsorption capacities to increase their efficacy in dye removal applications.

Table 4. Comparison of adsorption capacities of different adsorbents for methyl violet dye exclusion

Adsorbents	Adsorption capacity (mg/g)	References
Fe^{3+} cross-linked ternary carboxymethyl cellulose/polyaniline/TiO_2 photocomposites	159.08	Benhalima et al. (2024)
Polypyrrole-modified biopolymers	88.5	Benhalima et al. (2023b)
Ag-NPs-loaded cellulose derived from peanut-husk agro-waste	7.0928	Aljeddani et al. (2023)
Pectin hydrogel@Fe_3O_4-bentonite	909.091	Beigi et al. (2023)
Cationic ion exchange resin Amberlite®IRC-50	10.0	Bensalah et al. (2023)
Bio-adsorbent from date seeds	59.5	Ali et al. (2022)
Coconut husk powder	454.54	Sultana et al. (2022)
Microporous coconut shell activated carbon	320.5	Kamdod and Kumar (2022)
Egg shell	25.73	Khadam et al. (2022)
Mesoporous aluminosilica monoliths	554.85	Al-Hazmi et al. (2022)
NaOH-activated aerva javanica leaf	315.2	AL-Shehri et al. (2021)
Activated carbon from lemon wood/Fe_3O_4 magnetic nanocomposite	35.3	Foroutan et al. (2021)
Phenolated alkali lignin/magnetite composite	6.42	Present Study

4. CONCLUSION

This study demonstrates that the phenolated alkali lignin/magnetite composite is an effective adsorbent for methyl violet, exhibiting excellent adsorption capacity and reusability. This adsorbent proves to be a practical and cost-effective solution for the treatment of methyl violet-contaminated wastewater. The equilibrium removal rate of methyl violet is recorded at 95.1%, with an adsorption capacity at equilibrium of 6.42 mg/g. The adsorption of methyl violet follows a pseudo-second-order kinetic model, and the Freundlich isotherm model. This suggests that the adsorption is multilayered, and the PAL/magnetite composite contains heterogeneous adsorption sites.

ACKNOWLEDGEMENTS

The College of Science at Technological University of the Philippines deserves the authors' sincere gratitude for providing the materials for the effective completion of this study.

REFERENCES

Aljeddani G, Alghanmi R, Hamouda R. Study on the isotherms, kinetics, and thermodynamics of adsorption of crystal violet dye using Ag-NPs-loaded cellulose derived from peanut-husk agro-waste. Polymers 2023;15(22):Article No. 4394.

Al-Hazmi G, Akhdhar A, Shahat A, Elwakeel K. Adsorption of Gentian violet dye onto mesoporous aluminosilica monoliths: Nanoarchitectonics and application to industrial wastewater. International Journal of Environmental Analytical Chemistry 2022. DOI: https://doi.org/10.1080/03067319.2022.2104641.

Ali N, Jabbar N, Alardhi S, Majdi H, Albayati T. Adsorption of methyl violet dye onto a prepared bio-adsorbent from date seeds: Isotherm, kinetics, and thermodynamics studies. Heliyon 2022;8(8):Article No. 10276.

AL-Shehri H, Almudaifer E, Alorabi A, Alanazi H, Alkorbi A, Alharthi F. Effective adsorption of crystal violet from aqueous solutions with effective adsorbent: Equilibrium, mechanism studies and modeling analysis. Environmental Pollutants and Bioavailability 2021;33(1):214-26.

Ayawei N, Angaye S, Wankasi D, Dikio E. Synthesis, characterization and application of Mg/Al layered double hydroxide for the degradation of congo red in aqueous solution. Open Journal of Physical Chemistry 2015;5(3):56-70.

Ayawei N, Ebelegi A, Wankasi D. Modelling and interpretation of adsorption isotherms. Journal of Chemistry 2017;2017:Article No. 3039817.

Beigi P, Ganjali F, Hassanzadeh-Afruzi F, Salehi M, Maleki A. Enhancement of adsorption efficiency of crystal violet and chlorpyrifos onto pectin hydrogel@Fe_3O_4-bentonite as a versatile nanoadsorbent. Scientific Reports 2023;13:Article No. 10764.

Benhalima T, Ferfera-Harrar H. Eco-friendly porous carboxymethyl cellulose/dextran sulfate composite beads as reusable and efficient adsorbents of cationic dye methylene blue. International Journal of Biological Macromolecules 2019;132:126-41.

Benhalima T, Ferfera-Harrar H, Lerari D. Optimization of carboxymethyl cellulose hydrogels beads generated by an anionic surfactant micelle templating for cationic dye uptake: Swelling, sorption and reusability studies. International Journal of Biological Macromolecules 2017;105(1):1025-42.

Benhalima T, Ferfera-Harrar H, Saha N, Saha P. Fe_3O_4 imbuing carboxymethyl cellulose/dextran sulfate nanocomposite hydrogel beads: An effective adsorbent for methylene blue dye pollutant. Journal of Macromolecular Science, Part A 2023a;60(6):442-61.

Benhalima T, Chicha W, Ferfera-Harrar H. Sponge-like biodegradable polypyrrole-modified biopolymers for selective adsorption of basic red 46 and crystal violet dyes from single and binary component systems. International Journal of Biological Macromolecules 2023b;253(8):Article No. 127532.

Benhalima T, Mokhtari M, Ferfera-Harrar H. Synergistic adsorption/photodegradation effect for effective removal of crystal violet dye and acetamiprid pesticide using Fe^{3+} cross-linked ternary carboxymethyl cellulose/polyaniline/TiO_2 photocomposites. Journal of Water Process Engineering 2024;57:Article No. 104670.

Bensalah J. Removal of the textile dyes by a resin adsorbent polymeric: Insight into optimization, kinetics and isotherms adsorption phenomenally. Inorganic Chemistry Communications 2024;161:Article No. 111975.

Bensalah B, Idrissi A, Faydy M, Doumane G, Staoui A, Hsissou R, et al. Investigation of the cationic resin as a potential adsorbent to remove MR and CV dyes: Kinetic, equilibrium isotherms studies and DFT calculations. Journal of Molecular Structure 2023;1278:Article No. 134849.

Canbaz G. Fe_3O_4@Granite: A novel magnetic adsorbent for dye adsorption. Processes 2023;11(9):Article No. 2681.

Casas N, Parella T, Vicent T, Caminal G, Sarrà M. Metabolites from the biodegradation of triphenylmethane dyes by Trametes versicolor or laccase. Chemosphere 2009; 75(10):1344-9.

Chaudhari A. Nitrobenzene oxidation for isolation of value added products from industrial waste lignin. Journal of Chemical, Biological and Physical Sciences 2016;6(63):501-13.

Chen J, Chen H. Removal of anionic dyes from an aqueous solution by a magnetic cationic adsorbent modified with DMDAAC. New Journal of Chemistry 2018;42:7262-71.

Chiban M, Soudani A, Sinan F, Persin M. Single, binary and multi-component adsorption of some anions and heavy metals on environmentally friendly *Carpobrotus edulis* plant. Colloids Surf B Biointerfaces 2011;82(2):267-76.

Fang L, Wu H, Shi Y, Tao Y, Yong Q. Preparation of lignin-based magnetic adsorbent from kraft lignin for adsorbing the congo red. Frontiers in Bioengineering and Biotechnology 2021;9:Article No. 691528.

Foroutan R, Mohammadi R, Farjadfard S, Esmaeili H, Ramavandi B, Sorial G. Eggshell nano-particle potential for methyl violet and mercury ion removal: Surface study and field application. Advanced Powder Technology 2019;30(10):2188-99.

Foroutan R, Peighambardoust S, Peighambardoust S, Pateiro M, Lorenzo J. Adsorption of crystal violet dye using activated carbon of lemon wood and activated carbon/Fe_3O_4 magnetic nanocomposite from Aqueous Solutions: A kinetic, equilibrium and thermodynamic study. Molecules 2021; 26(8):Article No. 2241.

Kamdod A, Kumar M. Adsorption of methylene blue, methyl orange, and crystal violet on microporous coconut shell activated carbon and its composite with chitosan: Isotherms and kinetics. Journal of Polymers and the Environment 2022;30:5274-89.

Khadam S, Javed T, Jilani M. Adsorptive exclusion of crystal violet dye from wastewater using eggshells: Kinetic and thermodynamic study. Desalination and Water Treatment 2022;268:99-112.

Liu G, Liao L, Dai Z, Qi Q, Wu J, Ma L, et al. Organic adsorbents modified with citric acid and Fe_3O_4 enhance the removal of Cd and Pb in contaminated solutions. Chemical Engineering Journal 2020;39:Article No. 125108.

Liu L, Luo X, Ding L, Luo S. Application of nanotechnology in the removal of heavy metal from water. In: Liu L, Luo X, Ding L, Luo S, Deng F, editors. Nanomaterials for Nanomaterials for the Removal of Pollutants and Resource Reutilization. Elsevier; 2019. p. 83-147.

Meng X, Scheidemantle B, Li M, Wang Y, Zhao X, Toro-González M, et al. Synthesis, characterization, and utilization of a lignin-based adsorbent for effective removal of azo dye from aqueous solution. ACS Omega 2020;5(6):2865-77.

Panamgama A, Peramune P. Coconut coir pith lignin: A physicochemical and thermal characterization. International Journal of Biological Macromolecules 2018;113:1149-57.

Ringot D, Lerzy B, Chaplain K, Bonhoure J, Auclair E, Larondelle Y. In vitro biosorption of ochratoxin A on the yeast industry by-products: Comparison of isotherm models. Bioresource Technology 2007;98(9):1812-21.

Saini R. Textile organic dyes: Polluting effects and elimination methods from textile waste water. International Journal of Chemical Engineering Research 2017;9(1):121-36.

Sharma J, Sharma S, Soni V. Classification and impact of synthetic textile dyes on Aquatic Flora: A review. Regional Studies in Marine Science 2021;45:Article No. 101802.

Sultana S, Islam K, Hasan M, Khan H, Khan M, Deb A, et al. Adsorption of crystal violet dye by coconut husk powder: Isotherm, kinetics and thermodynamics perspectives. Environmental Nanotechnology, Monitoring and Management 2022;17:Article No. 100651.

Taleb F, Ammar M, Mosbah M, Salem R, Moussaoui Y. Chemical modification of lignin derived from spent coffee grounds for methylene blue adsorption. Scientific Reports 2020;10:Article No. 11048.

Touihri M, Guesmi F, Hannachi C, Hamrouni B, Sellaoui L, Badawi M, et al. Single and simultaneous adsorption of Cr (VI) and Cu (II) on a novel Fe_3O_4/pine cones gel beads nanocomposite: Experiments, characterization and isotherms modeling. Chemical Engineering Journal 2021;416:Article No. 129101.

Wang T, Jiang M, Yu X, Niu N, Chen L. Application of lignin adsorbent in wastewater Treatment: A review. Separation and Purification Technology 2022;302:Article No. 122116.

You X, Zhou R, Zhu Y, Bu D, Cheng D. Adsorption of dyes methyl violet and malachite green from aqueous solution on multi-step modified rice husk powder in single and binary systems: Characterization, adsorption behavior and physical interpretations. Journal of Hazardous Materials 2022; 430:Article No. 128445.

Younesi-Kordkheili H, Pizzi A. A Comparison among lignin modification methods on the properties of lignin-phenol-formaldehyde resin as wood adhesive. Polymers 2021; 13(20):Article No. 3502.